

Nanostructured commercially pure titanium for development of miniaturized biomedical implants

4.3

R.Z. Valiev[†], I. Sabirov^{†,‡}, E.G. Zemtsova[†], E.V. Parfenov*, L. Dluhos[§], T.C. Lowe[¶]*

*Ufa State Aviation Technical University, Ufa, Russia, [†]St. Petersburg State University, St. Petersburg, Russia, [‡]IMDEA Materials Institute, Getafe, Madrid, Spain, [§]Timplant s.r.o., Sjednocení, Ostrava, –Polanka, Czech Republic, [¶]George S. Ansell Dept. of Metallurgical and Materials Engineering, Colorado School of Mines, Golden, Colorado, United States

4.3.1 Introduction

Commercially pure Ti (CP Ti) is known to be highly biocompatible with human bone tissue, making it suitable for orthopaedic and dental applications [1–4]. Its corrosion resistance in biological environments is superior to most medical metals because of its stable and adherent surface layer of TiO₂ [1,5]. Titanium also has an elastic modulus that is half that of stainless steel or Co-Cr alloys, which reduces its propensity to cause stress shielding and associated bone resorption. Titanium has other advantages, including being lighter in weight due to its low density and being non-ferromagnetic so that patients with titanium implants are not restricted from diagnosis by magnetic resonance imaging and computed tomography techniques [6,7]. Unfortunately, both the tensile strength and fatigue endurance limit of conventional CP Ti are relatively low, limiting its use in high-load structural applications. The compactness of implant system components, especially for maxillofacial hardware, is a desirable attribute [7–9]. However, maxillofacial bone replacements must sustain loads between 200 and 700 N [5]. Similarly, a 1 mm diameter screw may experience stresses of 900 MPa, which is higher than the ultimate tensile strength of CP Ti [10]. Higher-strength alloys are clearly needed for such applications [1,5,8]. The addition of alloying elements can significantly improve the mechanical properties of titanium, but the most commonly used alloying elements—aluminum and vanadium—are non-specific mutagens and may have toxic effects. While Ti alloys with these elements are used in medical implants, the virtues of replacing these alloys with alternative alloys that do not contain vanadium or aluminum is a current research frontier. Efforts to reduce the use of toxic elements have resulted in the adoption of the vanadium-free Ti-6Al-7Nb alloy in some applications and promoted the evaluation of other alternative alloys [6–8]. Another promising way to enhance the strength of titanium is nanostructuring by severe plastic deformation (SPD) to dramatically reduce

grain size [9–13]. Our recent studies have shown that a variation of equal-channel angular pressing (ECAP) to make it continuous by implementing a conform-like method (i.e., the ECAP-conform (ECAP-C)), can be combined with subsequent drawing to produce long rods with nanoscale structures [14–16]. Nanostructuring of titanium increases strength and fatigue resistance to levels that exceed those reported for Ti-6Al-4V ELI [17–19]. The additional strength and fatigue resistance of nanostructured titanium make it possible to miniaturize medical devices.

This chapter focuses on the results that support the possibility of obtaining high-strength nanostructured pure titanium bars and semifinished products with improved fatigue resistance through the use of the ECAP-C technology. The superior properties of nanostructured titanium further enable the development of improved designs for medical products. The examples of making and using thin implants with improved design for dentistry and orthopedics are presented.

4.3.2 Material and methods

Rods of Grade 4 titanium at 12 mm in diameter, meeting all the specifications of the ASTM F67 standard for medical implants, were used in the study reported herein. The material impurity data was (in wt%) 0.050% C, 0.20% Fe, 0.35% O₂, 0.007% N, and 0.0020% H with the average grain size of the titanium rods in as-received condition equal to ~ 25 μm. The rods were nanostructured via ECAP-C and drawing. The former processing technique is a comparatively recent modification of the standard ECAP method [14,16,19]. In the course of this process, a workpiece is forced through an ECAP die in a manner analogous to the conform process; however in this case an upgraded ECAP design is applied for nanostructured materials to be produced with repeat passes.

As-received Grade 4 Ti rods were subjected to ECAP-C in a die-set with a 120-degree intersection angle Φ through the B_c route. Subsequent drawing was carried out to a reduction ratio of 85%. The deformation temperature was equal to 200°C. The processing details are presented in Refs. [19,20]. The final processed rods had a length of 3 m with a diameter from 3 to 6 mm.

The microstructure was analyzed by means of optical as well as transmission electron microscopy (TEM) in a JEOL JEM 2100 TEM with acceleration voltage 200 kV. Prior to this, the samples were mechanically polished and etched in a chemical solution (4% hydrofluoric acid, 20% perchloric acid, and 76% distilled water) for surface treatment. The samples for TEM were prepared by electrospark machining, mechanically thinned down to 100 μm, and then electrolytically polished on a “Tenupol-5” device. Electropolishing was performed with 5% perchloric acid, 35% butanol, and 60% methanol chemical solution.

The cylinder-shaped samples, 3 mm in diameter and of 15 mm gauge length, were tensile tested at room temperature in an INSTRON-type device with a primary strain rate of 10^{-3} s^{-1} . The tensile axis was parallel to the rod axis. Stress-controlled fatigue tests at ambient temperature were carried out to characterize the behavior of nanostructured (NS) and conventional coarse grain (CG) CP titanium at a load ratio

of $R (\sigma_{\min}/\sigma_{\max}) = -1$. Rotational bending testing with a frequency of 50 Hz was also performed.

Surfaces of mechanically polished CG and NS samples of Grade 4 Ti were acid etched in 30% $\text{HNO}_3 + 3\% \text{HF} + \text{H}_2\text{O}$ for 20 min. Analysis of the surface of the etched specimens was performed on an Olympus GX51 optical microscope and JEOL JSM 6390 scanning electron microscope (SEM). Surface topography was examined with an LSM-5-Exciter laser scanning microscope (LSM). Surface profiles were analyzed to determine the surface roughness parameter R_a and the size of etching dimples.

4.3.3 Design of miniaturized implants

4.3.3.1 Dental thin implants

Nanoimplant dental implants are produced within the frame of research of the dental implant system Nanoimplant from pure nanostructured Grade 4 Ti rods processed by the ECAP-C on CNC machines in diameters of 2.0, 2.4, and 3.5 mm with the intraosseal part length of 8, 10, 12, and 14 mm by the company “Timplant” s.r.o., Czech Republic. The implant is characterized by an etched, threaded, and tapered intraosseal part with a polished gingival part and prosthetic cone top with interior thread above it and with an antirotation crown element. High primary stability is achieved by an enhanced thread design with a self-drilling thread groove. Special etching provides the surface roughness.

Nano-CP Ti contains neither toxic alloying elements (such as V or Al) nor elements labeled as allergens (such as Ni, Co, or Cr). It is characterized by high strength, enabling the production of thin implants. The clinical performance of 2.4 mm Nanoimplants was evaluated on the basis of a two-year statistical observation by five surgeon dentists both from state-owned dental surgeries as well as privately run dental surgeries in the Czech Republic [20].

4.3.3.2 Geometrical parameters of nano-Ti miniplates

Simple rules are used to redesign devices to address the effects of changing materials, such as substituting nanostructured CP Ti for CG Ti. Fatigue performance must be retained, carefully considering the possibility of changing device cross-sectional dimensions. The minimum cross-sectional area A of a plate subject to surface tension and compression by reverse bending is given by:

$$A \geq F_{\max}/\sigma_f \quad (4.3.1)$$

and for bending, the axial resistance moment is:

$$W \geq Mb_{\max}/\sigma_f \quad (4.3.2)$$

where σ_f is the fatigue endurance limit and F_{\max} and Mb_{\max} are the maximum applied force and bending moment, respectively.

In a recent study [35], a “Conmet” company miniplate made of CP Ti [21], as specified by ASTM F 67, was used as the starting point for redesigning the product dimensions for making a nanostructured CP Ti miniplate. The cross-section area for the redesigned plate was computed using measurements of the fatigue endurance limit for coarse-grained Grade 4 Ti $\sigma_{f(\text{CG})}$ and nanostructured Grade 4 Ti $\sigma_{f(\text{NS})}$ (Section 4.3.2). The fatigue strength ratio K_r was calculated as:

$$K_r = \sigma_{f(\text{CG})} / \sigma_{f(\text{NS})} \quad (4.3.3)$$

This ratio K_r was applied to scale the design criteria in Eqs. (4.3.1), (4.3.2), considering tension/compression and bending mode loadings to determine the appropriate size for a nanostructured Grade 4 Ti plate, according to Eqs. (4.3.4), (4.3.5):

$$A_{(\text{NS})} \geq A_{(\text{CG})} \times K_r \quad (4.3.4)$$

for bending:

$$W_{(\text{NS})} \geq W_{(\text{CG})} \times K_r \quad (4.3.5)$$

Because plates more commonly support bending loads [1], the bending strength of miniplates made of conventional CG Ti and nanostructured Ti were compared [22,23]. In addition, the fatigue strength of miniplates was compared through testing with an ElectroPuls E3000 system [23]. Cyclic 3 mm displacements were applied at 30 Hz to determine the number of cycles to failure N . Triplicate tests were performed. The miniplate was fixtured as a cantilever so that the axial resistance moment is given by [24]:

$$W = \frac{bh^2}{6} \quad (4.3.6)$$

where b and h are the width and thickness of the miniplate, respectively. The bending moment Mb (bending strength) can then be determined by substituting σ_f and W from Eq. (4.3.6) into Eq. (4.3.2) for conventional and nanostructured miniplates.

4.3.4 Nano-Ti studies and implant characterization

4.3.4.1 Microstructure and mechanical properties of nano-Ti

The ECAP-C processing combined with drawing led to significant grain refinement from 25 μm to 150 nm, resulting in an equiaxed grain microstructure (see Fig. 4.3.1).

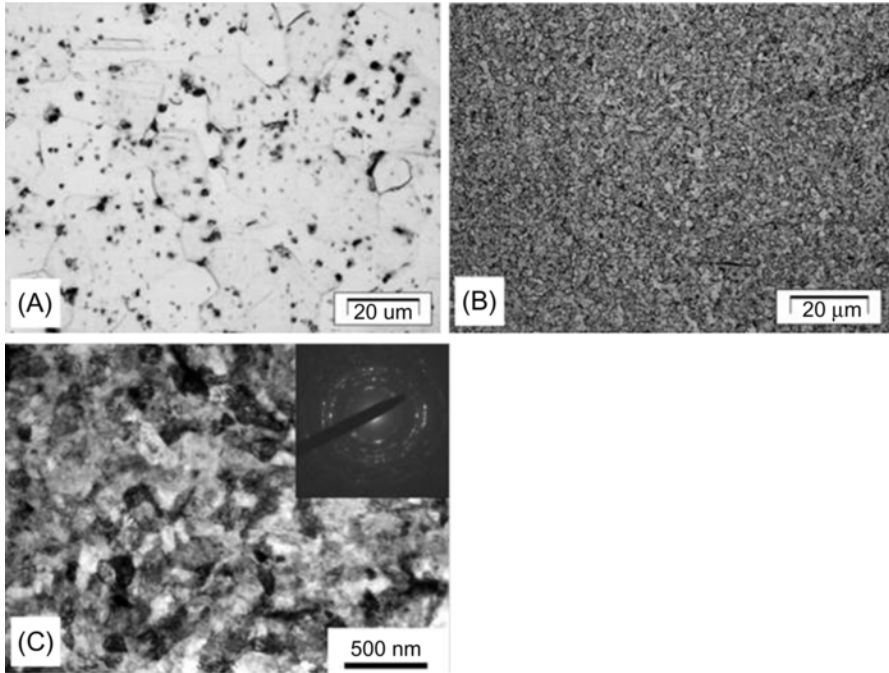


Fig. 4.3.1 Microstructure of Grade 4 CP Ti: (A) the initial coarse-grained rod; (B) and (C) cross-section of the rod after ECAP-C + drawing (optical (A), (B), and TEM (C) images).

It can be concluded from the SAED pattern, Fig. 4.3.1C, that the microstructure comprised mainly high-angle grain boundaries. A similar microstructure can be generated in disks of CP Ti by different SPD processing techniques such as high-pressure torsion (HPT) (see [27] for more details). The main task of the present research was to investigate properties of a homogeneous ultrafine-grained structure in 3 m rods to provide experimental manufacturing of implants and supply enough material for careful characterization of the biomedical and mechanical features. It is seen from Table 4.3.1 that the strength of the nanostructured Ti by a factor of two exceeds that of its conventional coarse-grained counterpart. Moreover, it was possible to achieve this improvement without significant degradation of material ductility, which usually takes place when conventional metal-forming techniques such as rolling or drawing are employed.

The ECAP processing combined with drawing also increases ultimate tensile strength (UTS) in Ti by a factor of two. A clear strength growth is known to be observed after conventional deformation processing methods (rolling, drawing, swaging, etc.) with the increase of the accumulated strain and microstructure refinement; however, a noticeable reduction in ductility occurs as well. This happens because such processing techniques lead to a subgrain kind of microstructure, distinguished

Table 4.3.1 Mechanical properties of conventionally processed and nanostructured Grade 4 Ti produced by ECAP-C and drawing. Data on Ti-6Al-4 V ELI alloy are presented to compare

Processing/ treatment terms	UTS (MPa)	YS (MPa)	Elongation (%)	Reduction of area (%)	Fatigue strength at 10^7 cycles
Conventional Ti (as received)	700	530	25	52	340
Nano-Grade 4	1330	1267	11	48	620
Annealed Ti-6Al-4V ELI	940	840	16	45	530

by pronounced metallographic and crystallographic textures along with low fraction of grain boundaries with high angles.

In addition, SPD processing enables the creation of a UFG structure characterized by homogeneity, a vast amount of high-angle grain boundaries, and a scarcity of strong texture. Such an ultrafine-grained microstructure like this ensures the combination of high strength and sufficient ductility through the Hall-Petch relation [25–27], as the grain boundary origin in UFG materials is extremely relevant in identifying the level of mechanical properties. Publications focused on UFG Ti [27,28] showed that the formation of high-angle, nonequilibrium grain boundaries can ensure intergranular sliding processes in the course of rigid plastic deformation even at room temperature, significantly affecting ductility and formability of the material. The fraction of high-angle grain boundaries in the UFG Ti increases with accumulated strain and results in an alteration of the basic deformation mechanisms owing to the growing contribution of grain boundary sliding and rotation [10,25].

The present research proves that an ultrafine-grained structure formation in the course of SPD in Ti also results in a significant improvement of fatigue performance in comparison with the original condition. It increases from 340 MPa in the coarse-grained material to 600 MPa after ECAP-C and drawing (Table 4.3.1). The same tendency was demonstrated in earlier research using conventional ECAP [29,30]. Thus, the fatigue limit of nanostructured CP titanium at 10^7 cycles is nearly twice that of conventional CP titanium and is higher than that of the Ti-6Al-4V alloy [6,31]. The ratio $\sigma_{-1}/\sigma_{UTS} = 0.47$ is relatively equal to the same value for CG Ti. The fatigue strength of CP titanium can be correlated with tensile strength, it being a characteristic of Ti in contrast to the metals with FCC lattice [30]. This to some degree could be the result of the complexity of dislocation cross slip in the HCP lattice, that is, the fatigue life of titanium is dependent on different parameters of UFG microstructure, the latter including grain size and shape as well as boundary type. Fatigue mechanisms may be related to grain boundaries whereas twinning has no pronounced contribution to the cyclic deformation of UFG Ti. Rods of SPD-processed

Grade 4 Ti demonstrate the formation of a homogeneous UFG structure with equiaxed grains in the transverse as well as longitudinal sections with mostly high-angle boundaries after ECAP-conform and subsequent drawing. The rods along the whole length have a homogeneous distribution of tensile characteristics, as demonstrated by the corresponding tests of samples extracted from the rods of various batches. The uniformity evaluation was carried out by the coefficient of variation in compliance with ASTM E8-95a.

According to the results shown in Table 4.3.1, the ECAP-conform of Ti combined with drawing combined with deformation processing of Ti using results in an effective combination of improved mechanical strength and ductility, thereby demonstrating the validity of the method. Combined thermomechanical treatment, including the method of ECAP-conform and drawing, is already being used by the “NanoMeT” company, and it provides the basis for the experimental manufacturing of nano-Ti rods with improved strength. This method was certified in compliance with ISO 9001:2008. Products of the company also satisfy the requirements of the GOST 26877-91 standard for medical implants [20,35].

The SPD technology development to produce nanostructured titanium characterized by improved mechanical properties allows for the fabrication of dental implants with smaller diameters [20]. The computational study [32,33] demonstrates that those narrow implants having a diameter of 2.4 mm are able to endure the same loads as the ones born by implants of the conventional design having a diameter of 3.5 mm manufactured from conventional Ti.

It needs to be mentioned that UFG pure Ti processed by ECAP or ECAP-C combined with drawing or swaging always shows the fiber crystallographic texture, where the basal plane and $\varphi 10 - 10^\circ$ direction are parallel to the rod axis [16,34]. Such texture is formed at the final stage of processing (i.e., during drawing or swaging) and can result in significant anisotropy of mechanical strength and ductility. Particularly, it was shown that the tensile yield strength of UFG CP Ti with a fiber texture is lower compared to its yield strength in the longitudinal direction, though it is still higher compared to the yield strength of conventional coarse-grained Ti [34]. This anisotropy of mechanical properties should be carefully considered in designing mini implants in order to avoid their deformation and fracture during service life.

4.3.4.2 *Nano-Ti plates for maxillofacial surgery*

In order to produce implants using nanostructured Ti, a plate designed by the “Conmet” company (Moscow, Russian Federation) for maxillofacial surgery was used [22], as is shown in Fig. 4.3.2.

According to formula (4.3.5), being aware of the values of the fatigue limit of coarse-grained and nanostructured Ti (see Table 4.3.1), it is possible to figure out the coefficient K_r and the axial resistance moment W . The minimum potential area of the cross-section of nano-Ti plates with preservation of the object's fatigue strength can therefore be determined. Table 4.3.2 demonstrates the outcome of the calculation of



Fig. 4.3.2 Image of a miniplate with six holes made from nanostructured Grade 4 Ti.

Table 4.3.2 Sizes of a base plate from CG and NS Grade 4 Ti [35]

Plate	Fatigue strength limit σ_f (MPa)	Strength ratio, K_r	Geometrical sizes of a plate				Axial resistance moment (W)
		$K_r = \sigma_{f(CG)}/\sigma_{f(NS)}$	Length, L (mm)	Area in the central part, A (mm ²)	Thick-ness, h (mm)	Width, b (mm)	$W = \frac{bh^2}{6}$ mm ³
Ti plate	340	0.6	46.4	2.7	0.9	3	0.40
Nano-Ti plate	620		46.4	2.1	0.7	3	0.25

the cross-section area of the nano-Ti plate [35]. Only the plate thickness is changed with the width and diameter the same as in the standard item.

So, a reduction of plate thickness from 0.9 to 0.7 mm satisfies the terms of ratios (4) and (5). Using the fatigue endurance limit values (σ_f) for Grade 4 Ti, taking into account the axial resistance moment W values of the plate with standard and reduced sizes, the maximum bending moment Mb_{\max} (bending strength) is determined in accordance with the ratio (2), which equals 140 MPa for CG Ti and 145 MPa for nano-Ti. This demonstrates that the reduced cross-section area does not necessarily result in the plate strength reduction while bending. Fig. 4.3.3 shows the experimental values of the fatigue life of plates following bending tests.

The standard plates have endured $17,000 \pm 500$ cycles while the plate with the reduced cross-section made from nanostructured Ti could withstand a greater number

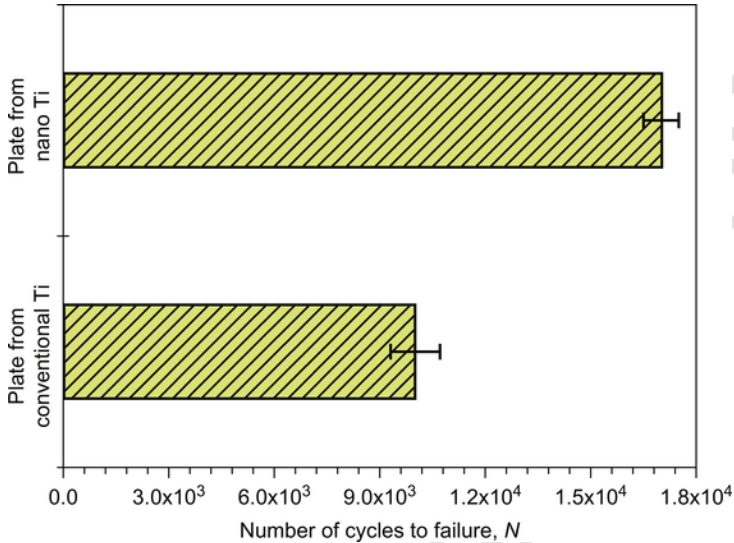


Fig. 4.3.3 Fatigue life of the standard plate and a plate from nano-Ti with a reduced cross-section area [35].

of cycles to failure ($105,000 \pm 800$). This result points to an enhancement of bending strength of the plate from nano-Grade 4 Ti. So it has a significant advantage over the standard item manufactured from coarse-grained Ti.

4.3.4.3 Nano-Ti dental implants

The reduced radius of an implant allows for reducing medical interference, therefore trauma related to implantation becomes much smaller. Implants with a reduced radius can be installed in patients with a thin alveolar bone while in such cases the use of a conventional CG Ti implant is not possible or necessitates extra intervention with subsequent bone augmentation [20]. Thin nanoimplants with a diameter of intraosseal part of 2.0 mm also have their application in dental orthodontics.

Nanoimplants are indicated in the cases where there is a lack of transversal dimension of the processus alveolaris, meaning a narrow alveolus within the range of 4.5–6 mm. In case the alveolus width is of 6 mm or more, the implant with a diameter of 3.5 mm is used. If the alveolus width is below 6 mm, a nanoimplant with a diameter of 2.4 mm is applied. For a very narrow alveolus below 4.5 mm, a nanoimplant with a diameter of 2.0 mm is used or bone splitting and insertion of an implant with possible augmentation (Fig. 4.3.4).

The indicative group for use of a diameter of 2.0 mm are the situations of insufficient mesiodistal interdental and interradicular dimension that fall into the dental field of orthodontics [36].

Better biological properties of nanoimplants in comparison to CP Ti implants have been demonstrated by a number of tests performed by the evaluation of cell

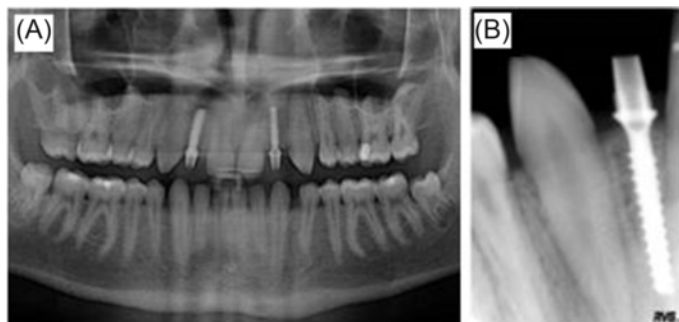


Fig. 4.3.4 2.0 mm diameter Nanoimplant (www.timplant.cz/en/) from nanostructured Grade 4 Ti in a panoramic X-ray radiograph after surgery (A), the right one, and the control radiograph obtained after incorporation of the implant (B).

proliferation on the surface of solid materials. In these tests, the cell proliferation velocity on the surface of nano Ti and CP Ti was compared after chemical etching. Etching of the samples for testing was performed using the same technology as for the manufacture of nanoimplants [37,38].

Quicker osteointegration and good primary retention of nanoimplants allow their full load immediately after their application, even in 70%–80% of cases. Primary implant retention in bone depends predominantly on the geometry of the intraosseous portion of the implant and on the shape of the tool for wound preparation.

A set of 250 patients to whom a total of 491 nanoimplants with a diameter of 2.4 mm were applied were monitored for 2 years. Out of that, 471 implants, or 96%, were immediately loaded implants in < 48 h ($t < 48$ h). Of these, seven implants were loaded within 7 days of implantation. From a total of 491, 11 implants were explanted. The overall success rate of the Nanoimplant implants is 97.9%. If it is generally possible to consider the success of the implants since their introduction, load by prosthetics, and retention for three or more years, the 100% success of implant retention on the set of 500 implants is rather theoretical.

The most frequently used prosthetic works on nanoimplants according to the above set are bridges of the size from 2 to 4 implants. The number of implants in these bridges is 292 (61.7%) while 35 implants (7.4%) were used to replace individual teeth as a solo pillar.

Those values are far smaller than the ones that are commonly found in dental practice [39].

Complications were caused by the processes of tissue inflammation around the implant, which might have led to a progressive destruction of the bone tissue around the implant. Various patients may have different reactions of living tissue and therefore, unfortunately, such cases are still encountered in modern dentistry. The reduction of such cases is possible by creating bioactive coatings on the implant surface, which may intensify the recovery of surrounding bone tissue and enhance implant

biocompatibility. The creation and study of bioinert and bioactive coatings on nanotitanium implants is still underway.

Nano-Ti with UTS around 1255 MPa was used for the production of 2.4 mm nanoimplants. The diameter of 2.4 mm represents 66% of the total number of 9000 applied nanoimplants, mostly in the Czech Republic. The stated strength of nano-Ti is sufficient for the given type of implant also from the viewpoint of risk, which is almost negligible thanks to calculations of the strength of implants or of real loading of the 2.4 mm implants. This has been evidenced by the fact that, during the past 10 years, we did not see a single case of breakage, bending, or other damage to the implant due to the load or use in the mouth.

The nanoimplants with a diameter of 3.5 mm are implanted into places with sufficient bone size and also into places after tooth extraction for immediate implantation. They are also manufactured from nano-Ti with UTS of 1255 MPa, not for ensuring their strength but for enabling faster osteointegration.

4.3.5 Surface modification of nano Ti implants

Surface properties are an important aspect of an implant design to ensure effective osseointegration. Pure Ti has very low bioactivity (i.e., bioinert material) and does not bond directly to the human bone [33]. As a result, the implant can shift and loosen during service life. A significant body of research has shown that grain refinement down to the nanoscale in CP Ti can stimulate various bone-forming cell types to adhere and proliferate with increased efficiency [40–44]. Additional surface modification can further improve the bioactivity of implants made from UFG Ti. Two main approaches of surface modifications can be noted: chemical etching and deposition of bioactive coatings [1,45–50]. In this overview we will focus on the first approach, namely, chemical etching, and then briefly discuss the second.

4.3.5.1 Chemical etching of nano-Ti implant surface

Acid treatment is often applied for removing contaminants from the surface (after mechanical treatment) and for making it straight in the process of finish machining [47]. As can be seen from [51,52], the implant can also be pretreated for the formation of a thick film of fluorides and hydrides on its surface upon reaction of hydrofluoric acid with oxide film TiO_2 , in which case such treatment uses a combination of acids $30\% \text{HNO}_3 + 3\% \text{HF} + \text{H}_2\text{O}$. While hydrides on the Ti surface may lead to the loss of ductility of the surface film, implementation of nitric acid in the solution substantially reduces a chance of free hydride formation [47]. That kind of treatment is very widespread in oral surgery dealing with dental problems, whereas it is subject to certain limitations when it comes to osteosynthesis. The reason for this is that the increase of surface roughness occurs with certain sacrifices to the fatigue resistance [1]. In recent research [45,50] the combination of acids was applied as the most general etching method to identify its impact on the topography of the nano-Ti surface. The research results revealed that nanostructuring in Ti leads to the formation of a

rougher surface after etching, which is stated by higher values of R_a , R_q , and R_{max} for nano-Ti (Table 4.3.3). Similar results have been obtained by multiple researchers [17,20,53–57], demonstrating that the peculiar relief on the nano-Ti surface contributed to higher rates of adhesion for both fibroblast [17,57] and preosteoblast [53,54] cells. In general, surface etching seems to have advantages in maxillofacial surgery when applied to artificial items made from nanostructured titanium to avoid contaminants and form a dense passivating film for solid osseointegration, whereas at the same time the formation of a rougher surface may affect the fatigue behavior of nano Ti [58]. In accordance with [19], the fatigue endurance limit of nano-Ti on smooth samples is significantly higher compared to CG Ti counterparts with similar roughness (600 and 350 MPa, respectively). Once samples have been etched, the R_a value is not $> 0.6 \mu\text{m}$ for either state of Ti (Table 4.3.3). Such a roughness value may have no effect on the fatigue strength of the material in the CG state as well as in the nanostructured state. Therefore, the items intended for maxillofacial surgery may be subjected to the applied etching regime. However, such an approach necessitates more thorough examination.

4.3.5.1.1 Results of LSM analysis

The analyses by LSM provide surface images of the CG and nano-Ti samples together with typical profiles along the scanning lines (Fig. 4.3.5). The surface relief

Table 4.3.3 AFM surface roughness analysis of as-received and nano-titanium sample surfaces

Scanning area $50 \times 50 \mu\text{m}$			
	R_a (μm)	R_q (μm)	R_{max} (μm)
Coarse-grained	0.44 ± 0.05	0.57 ± 0.07	3.7 ± 1.0
Nanostructured	0.56 ± 0.10	0.72 ± 0.067	5.6 ± 1.2

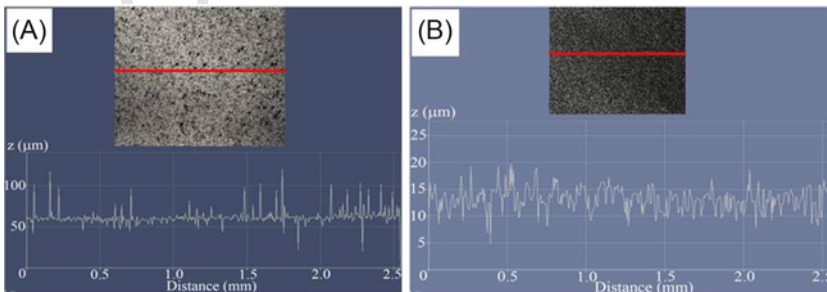


Fig. 4.3.5 General view of the surface and profile in the section (*red line*) of the CG (A) and UFG (B) Grade 4 Ti samples after etching in the mixture of acids for 20 min (LSM).

was statistically analyzed for higher values of the arithmetical mean roughness value (R_a) and true surface area (S_v) on the nano-Ti surface after etching. The histogram (see Fig. 4.3.6) demonstrates that R_a and S_v for nano-Ti are $1 \mu\text{m}$ and 0.035 mm^2 compared with these parameter values of $0.6 \mu\text{m}$ and 0.02 mm^2 for CG Ti, respectively.

4.3.5.1.2 Results of AFM analysis

Fig. 4.3.7A and C show typical representations of the surface relief made using atomic force microscopy (scanning area $50 \times 50 \mu\text{m}$). The relief profiles were scanned on a Nova «NT-MDT» software device and statistically analyzed for roughness parameters R_a , R_q , R_{max} in Table 4.3.3.

The parameter R_a for either state of Ti after being etched is 0.44 and $0.56 \mu\text{m}$, respectively, for CG and NS Ti (see Table 4.3.4). That parameter is identified as the peak average height on the surface profile. Yet it does not necessarily represent differential features of the relief. Particularly similar values of R_a can be found on the implant surfaces; however, their characteristics can be quite different [59]. The roughness parameter R_q is to a greater degree “sensitive” to surface variations because it is identified as the slight square deviation (amplitude) of peak heights and valleys depth from the midline [60]. The values of R_q for CG and UFG Ti differ more (0.56 and $0.72 \mu\text{m}$, respectively). The parameter R_{max} represents the highest peaks and the deepest valleys on the sample surface profile. This parameter is greatly different for CG and UFG samples (3.7 and $5.6 \mu\text{m}$, respectively).

4.3.5.1.3 Results of SEM analysis

Fig. 4.3.8 shows the scanning electron micrographs of the sample surface after etching. On the CG Ti surface, etch dimples can be seen, having an average size of approximately $3 \mu\text{m}$ (Fig. 4.3.8A). Unlike the coarse-grained sample, the surface of NS

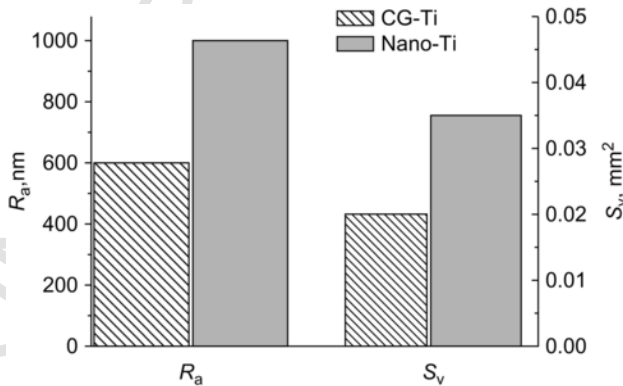


Fig. 4.3.6 The average arithmetic roughness value (R_a) and true area of the CG and UFG Grade 4 Ti sample surface (scanning area $S = 0.015 \text{ mm}^2$) after etching in the mixture of acids for 20 min.

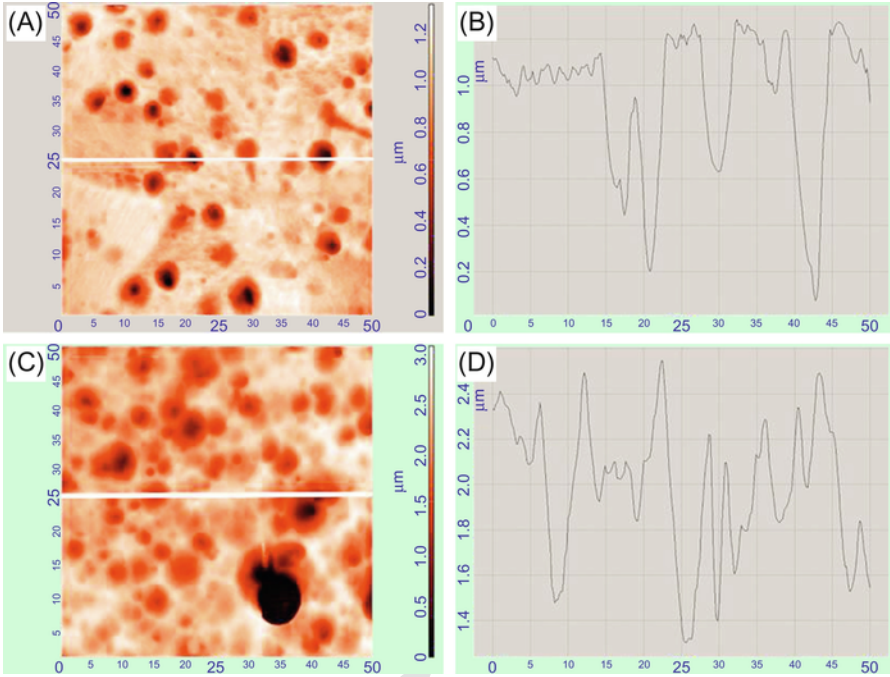


Fig. 4.3.7 Typical images of the surface topography of samples (scanning area $50 \times 50 \mu\text{m}$) (A, C) and profiles (B, D) of CG and UFG Grade 4 Ti after etching. (A, B) Surface of CG Ti (C, D) surface of nano-Ti. AFM.

Table 4.3.4 Key design parameters for bending tests of standard and pilot plates

Plate	Deflection δ (mm)	Elastic modulus $E \times 10^3$ (MPa)	Axial inertia moment, I (mm^4)	Axial resistance moment W (mm^3)	Applied force F_{max} (N)	Applied bending moment Mb_{max} (N ? mm)	Bending stress σ_{max} (MPa)
Standard plate	3	110	0.182	0.40	1.8	83.7	209
Nano-Ti plate	3	110	0.086	0.25	0.9	39.6	158

Ti is characterized by a higher density of dimples with sizes between 1 and $4 \mu\text{m}$ (Fig. 4.3.8B). A differing characteristic of dimples imaged by SEM on the surfaces of CG and NS Ti agrees with the profiles observed using the atomic force microscopy (see Fig. 4.3.7B and D). Significant differences in the microrelief observed

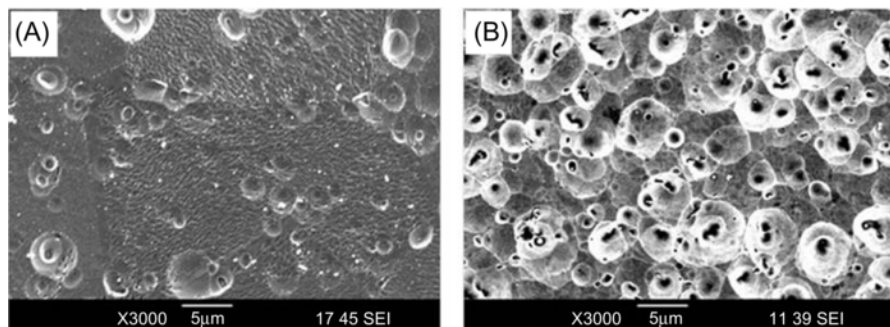


Fig. 4.3.8 Surface of CG and NS samples of Grade 4 Ti after mechanical polishing and etching in the mixture of acids 30% HNO_3 + 3% HF + H_2O for 20 min: (A) CG Ti surface; (B) nano-Ti surface. SEM images.

in the CG and NS states are under the influence of the increased density of intragranular boundaries and great density of defects in the NS material that make more active etching possible [61]. Topography research made using different methods (LSM, SEM, and AFM) shows a tendency for the formation of a particular relief after the nanostructured Ti surfaces have been etched. This can be marked both by higher roughness and greater density of etching dimples.

4.3.5.1.4 *Some notes on etching of UFG Ti*

It should be noted that the topography of etched surfaces is strongly determined by etching solution and etching time. Other solutions, such as acidic ($\text{H}_2\text{SO}_4/\text{H}_2\text{O}_2$) or basic ($\text{NH}_4\text{OH}/\text{H}_2\text{O}_2$) Piranha solutions, can also be utilized for etching CP Ti [62], resulting in different surface topographies. Manipulation with etching time can substantially modify the surface topography; this effect is more pronounced in the UFG Ti, as has been very recently demonstrated in [62]. In particular, it was found that etching with ammonia Piranha solution (unlike an acidic one) results in higher surface roughness and value of a particular surface area at insignificant etching times as well (Figs. 4.3.9 and 4.3.10). The acidic solution gives a noticeable increase of relief parameter only after etching for 2 h (Fig. 4.3.9). This was related to the less distinct passivation in the basic Piranha solution in comparison with the acidic one. Thus manipulation with both chemical etching solutions and etching time provides the tool for further surface design in the UFG CP Ti.

It should be noted that fiber texture present in the UFG Ti can result in its significant electrochemical anisotropy. Matykina et al. [63] have recently demonstrated that the HF-pickled nanostructured Ti shows a great distinction in roughness of the circumferential surface (made of basal planes) and transversal surface (made of prismatic planes) leading to greater release of Ti^{4+} ions from basal planes. However, the HF/ HNO_3 -pickling reveals electrochemical behavior of this kind in transverse as well as in circumferential surfaces of the nanostructured Ti rod. Then the electrochemical anisotropy is intensified in Hank's solution in the presence of D-glucose.

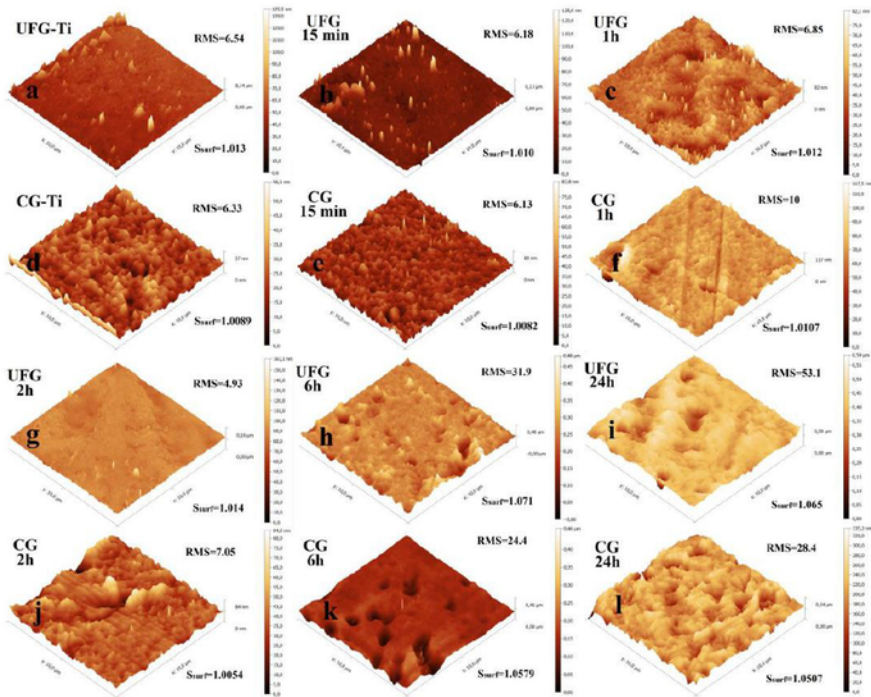


Fig. 4.3.9 Atomic force microscopy (AFM) surface topographies of the UFG and CG titanium etched in $\text{H}_2\text{SO}_4/\text{H}_2\text{O}_2$. Nonetched UFG-Ti (a), UFG-Ti etched 15 min (b), 1 h (c), nonetched CG-Ti (d), CG-Ti etched 15 min (e), 1 h (f), UFG-Ti etched 2 h (g), 6 h (h), 24 h (i), CG-Ti etched 2 h (j), 6 h (k), 24 h (l).

Therefore, HF-pickling of nanostructured Ti implants should be avoided in favor of HF/ HNO_3 -mixtures.

Analysis of Ti ion release into the human body from implants made of UFG Ti performed in [63] has shown its extremely low value, which is well below the cytotoxicity level of Ti, stated as 5 ppm [64]. Typically much higher concentrations of Ti ions were found in tissues near the implant made from conventional Ti alloys ($\leq 1000 \mu\text{m}$) than in blood or saliva [65].

4.3.5.2 Deposition of bioactive coatings on nano Ti implant surface

Biocompatible coatings can essentially facilitate integration of titanium implants into a human bone [66,67]. Therefore, research into the synthesis of biocompatible coatings integrating the inorganic (Ca-, P-containing phases) and organic (biologically active and bioinert molecules) components on titanium implants appears to be the topical state of the art [68,69].

The main crystalline component of a human bone is hydroxyapatite (HAp). This mineral is well studied [70], and is used in traumatology as a medication stimulating

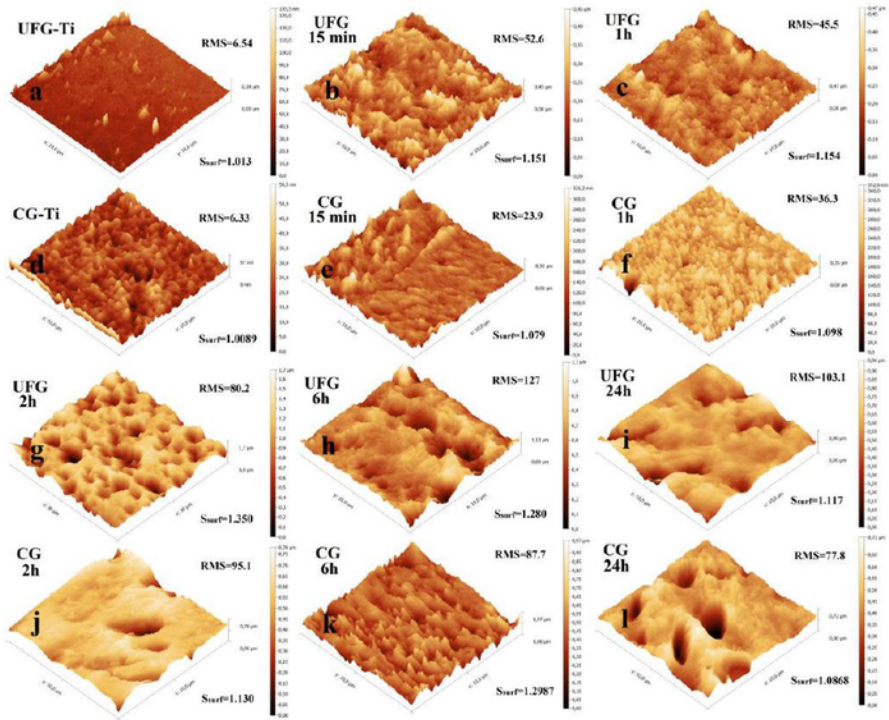


Fig. 4.3.10 AFM surface topographies of the UFG and CG Ti etched in $\text{NH}_4\text{OH}/\text{H}_2\text{O}_2$. Nonetched UFG-Ti (a), UFG-Ti etched 15 min (b), 1 h (c), nonetched CG-Ti (d), CG-Ti etched 15 min (e), 1 h (f), UFG-Ti etched 2 h (g), 6 h (h), 24 h (i), CG-Ti etched 2 h (j), 6 h (k), 24 h (l).

osteosynthesis. As a result, we can observe widely expanding attention paid to HAP containing coatings on titanium implants. A review [68] shows > 40 methods of calcium orthophosphate (including HAp) coating deposition on Ti implants: thermal spraying, chemical and electrochemical methods, vacuum, and other methods. The main problems still remain as low adhesion to the Ti substrate and low mechanical strength of HAP coatings [71]; therefore, the most beneficial methods are those forming HAP within a composite conversion coating.

During the last decade, significant attention has been paid to Ca- and P-containing coatings obtained by plasma electrolytic oxidation (PEO) [72–75]. The PEO process is an expansion of traditional anodizing into the high voltages up to 600 V; these voltages promote microdischarges within the coating (Fig. 4.3.11A); this results in its resolidifying and intensive growth [76,77]. This method is applicable to both CG and UFG titanium [78–80]. The coatings obtained by this method contain stable titania (rutile and anatase) tightly attached to the surface because of the process mechanism, including electrochemical oxidation and numerous melting and crystallizing events at the microdischarge sites [81–83]. This coating formation

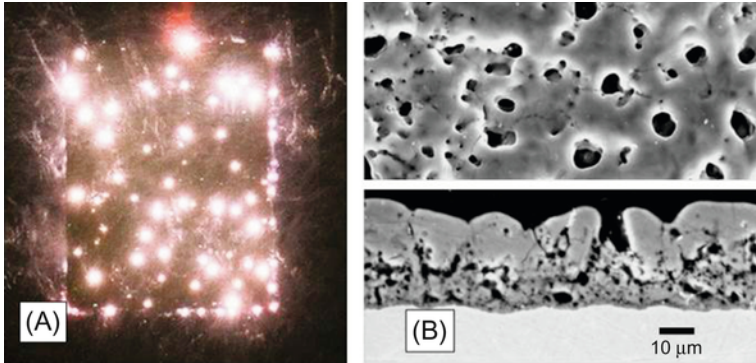


Fig. 4.3.11 Photographs of microdischarges on the sample surface during the PEO process (A); SEM image of PEO Ca- and P-containing coating on titanium, top view (above) and cross-section (below) (B) [76,84].

mechanism helps to develop coatings with regulated porosity with a pore size from 0.1 to 10 μm (Fig. 4.3.11B) [84]. This coating morphology provides a gradual change of the elasticity modulus from the metallic implant to the bone [85]; this enhances their biomechanical compatibility. The high surface area of the PEO coating promotes osteoblast attachment on the implant surface [86,87]. Applying varying pulse polarity during PEO and the introduction of bioactive particles into the electrolyte helps to incorporate the anions and cations of the electrolyte into the coating; this provides Ca- and P-containing bioactive crystalline phases within the coating: hydroxyapatite, tricalciumphosphate, tetracalciumphosphate, and perovskite [88,89]. Adhesion of the PEO coatings is higher than of other coating types [90].

The fundamental problems of *in vivo* coating compatibility are insufficiently investigated, despite recent studies [80,91,92]. Moreover, the fundamental question—which *in vitro* test would most correspond to in the *in vivo* situation for the PEO coatings in Ti in different structural states—still remains, and this answer is highly demanded.

4.3.6 Conclusions

As is clear from the results outlined in this chapter, nanostructured Grade 4 titanium appears to be material with a very high potential for medical applications. It is composed of elements that could not even theoretically cause harm to the body. It should be noted that nanostructured CP Ti also imparts good machinability. Additional research on nanostructured Ti is merited to achieve even greater ultimate strength and yield strength and for developing a means to reduce the effective the modulus of elasticity that could come close to the modulus of elasticity of the jawbone [32].

The results presented show that the ECAP-C with subsequent drawing provides new opportunities in the development of nanostructured Ti, providing the ability to uniformly enhance the strength in long rods that can be machined into dental im-

plants and other devices for medical applications. Evidence from the manufacture and clinical trial of dental implants has shown that enhanced designs with smaller diameters of 2.4 and 2.0 mm have been effectively inserted into thousands of human bodies for > 11 years.

Nanostructuring of CP Ti by SPD processing produces a material with mechanical properties superior to those of Ti-6Al-4V. The application of nano-Ti in maxillofacial surgery can be promising for producing miniature implant designs, in particular plates that will endure the same loads as conventional items.

Chemical etching and deposition of bioactive coatings can be utilized for surface modification in nanostructured Ti. Nanostructured CP Ti with modified surfaces can show improved functional properties such as improved surface bioactivity and reduced Ti ion release into the human body. This makes nanostructured Ti an attractive material for manufacturing implants. Nevertheless, biological *in vitro* studies are necessary to clarify the clinical significance of these research results.

Acknowledgments

The authors acknowledge the Russian Ministry for Education and Science for funding through Contract No. 14.B25.31.0017 on June 28, 2013. This has also been supported in part by grant No. 6.37.204.2016 from St. Petersburg State University.

References

- [1] D.M. Brunette, P. Tengvall, M. Textor, P. Thomsen, *Titanium in Medicine*, Springer-Verlag, Berlin, 20011019.
- [2] L.A. Assael, D.W. Klotch, P.N. Manson, J. Prein, B.A. Rahn, W. Schilli, in: J. Prein (Ed.), *Manual of Internal Fixation in the Cranio-Facial Skeleton*, Springer, Berlin, 1998, p. 227.
- [3] M.E. Müller, M. Allgöwer, R. Schneider, H. Willenegger, *Manual of Internal Fixation*, third ed., Springer, Berlin Heidelberg, 1991750.
- [4] M. Long, H.J. Rack, *Biomaterials* 19 (18) (1998) 1621.
- [5] N. Soumya, B. Banerjee, *Materials for medical devices*, in: R. Narayan (Ed.), *ASM Handbook*, Vol. 23, ASM International, Materials Park, OH, USA, 2012, pp. 6–17.
- [6] M. Niinomi, *Biologically and mechanically biocompatible titanium alloys mater*, *Transfusion* 49 (10) (2008) 2170.
- [7] M. Geetha, A.K. Singh, R. Asokamani, A.K. Gogia, *Ti based biomaterials, the ultimate choice for orthopaedic implants—a review* *Prog. Mater. Sci.* 54 (2009) 397.
- [8] M. Niinomi, *Recent metallic materials for biomedical applications*, *Metall. Mater. Trans. A* 32 (2001) 477.
- [9] R.Z. Valiev, R.K. Islamgaliev, I.V. Alexandrov, *Bulk nanostructured materials from severe plastic deformation*, *Prog. Mater. Sci.* 45 (2000) 1.
- [10] R.Z. Valiev, *Nanostructuring of metals by severe plastic deformation for advanced properties*, *Nat. Mater.* 3 (2004) 511.
- [11] M.J. Zehetbauer, Y.T. Zhu (Eds.), *Bulk Nanostructured Materials*, WILEY-VCH Verlag GmbH & Co. KGaA, Weinheim, 2009, p. 850.
- [12] Y. Estrin, A. Vinogradov, *Extreme grain refinement by severe plastic deformation: a wealth of challenging science*, *Acta Mater.* 61 (2013) 782.

- [13] T.G. Langdon, Twenty five years of ultrafine-grained materials: achieving exceptional properties through grain refinement, *Acta Mater.* 61 (2013) 7035–7059.
- [14] G.I. Raab, R.Z. Valiev, T.C. Lowe, Y.T. Zhu, Continuous processing of ultrafine grained Al by ECAP-conform, *Mater. Sci. Eng. A* 382 (2004) 30–34.
- [15] R.Z. Valiev, T.G. Langdon, Principles of equal-channel angular pressing as a processing tool for grain refinement, *Prog. Mater. Sci.* 51 (2006) 881.
- [16] D.V. Gunderov, A.V. Polyakov, I.P. Semenova, G.I. Raab, A.A. Churakova, E.I. Gimaltdinova, I. Sabirov, J. Segurado, V.D. Sitdikov, I.V. Alexandrov, N.A. Enikeev, R.Z. Valiev, Evolution of microstructure, macrotexture and mechanical properties of commercially pure Ti during ECAP-conform processing and drawing, *Mater. Sci. Eng. A* 562 (2013) 128.
- [17] R.Z. Valiev, I.P. Semenova, V.V. Latysh, H. Rack, T.C. Lowe, J. Petruzelka, L. Dluhos, D. Hrusak, J. Sochova, Nanostructured titanium for biomedical applications, *Adv. Eng. Mater.* 10 (8) (2008) B15.
- [18] T.C. Lowe, R.Z. Valiev, *Frontiers of bulk nanostructured metals in biomedical applications*, Chapter 1 in “Advanced Biomaterials and Biodevices,” A. Tiwari, A.N. Nordin, Wiley-Scrivener Publ., USA, 2014
- [19] I.P. Semenova, A.V. Polyakov, G.I. Raab, T.C. Lowe, R.Z. Valiev, Enhanced fatigue properties of ultrafine-grained Ti rods processed by ECAP-conform, *J. Mater. Sci.* 47 (2012) 7777–7781.
- [20] A.V. Polyakov, L. Dluhos, G.S. Dyakonov, G.I. Raab, R.Z. Valiev, Recent advances in processing and application of nanostructured titanium for dental implants, *Adv. Eng. Mater.* 17 (2015) 1865–1893, <https://doi.org/10.1002/adem.201500212>.
- [21] www.conmet.ru/e_main.html.
- [22] ISO 14602 Non-active surgical implants-Implants for Osteosynthesis particular requirements.
- [23] <http://www.instron.com/en/testing-solutions/by-test-type/simple-cyclic/orthopaedic-micro-implants>.
- [24] W. Beitz, K.H. Küttner, *Dubbel-Handbook of Mechanical Engineering*, Springer, Hong Kong, 1994.
- [25] R.Z. Valiev, I.V. Alexandrov, T.C. Lowe, Y.T. Zhu, Paradox of strength and ductility in metals processed by severe plastic deformation, *J. Mater. Res.* 17 (2002) 5.
- [26] F. Dalla Torre, R. Lapovok, J. Sandlin, P.F. Thomson, C.H.J. Davies, E.V. Pereloma, Microstructures and properties of copper processed by equal channel angular extrusion for 1–16 passes, *Acta Mater.* 52 (2004) 4819.
- [27] R.Z. Valiev, A.V. Sergueeva, A.K. Mukherjee, The effect of annealing on tensile deformation behavior of nanostructured SPD titanium, *Scr. Mater.* 49 (2003) 669–704.
- [28] R.Z. Valiev, A.P. Zhilyaev, T.G. Langdon, *Bulk Nanostructured Materials: Fundamentals and Applications*, John Wiley & Sons, Inc., Hoboken, NJ, 2013/2014456.
- [29] V.V. Stolyarov, I.V. Alexandrov, Y.R. Kolobov, M. Zhu, Y. Zhu, T. Lowe, in: X.R. Wu, Z.G. Wang (Eds.), *Proceedings of Fatigue*, Higher Education Press, 1999, pp. 1435–1440.
- [30] A.Y. Vinogradov, V.V. Stolyarov, S. Hashimoto, R.Z. Valiev, Cyclic behavior of ultrafine-grain titanium produced by severe plastic deformation, *Mater. Sci. Eng. A* 318 (2001) 163.
- [31] R. Boyer, G. Welsch, E. Collings (Eds.), *Materials Properties Handbook: Titanium Alloys*, ASM International, Materials Park, OH, 1994, p. 1998.
- [32] L. Dluhoš, J. Petruželka, Manufacturing of functional prototype of implantable medical appliance. Final project report, Project ViNaT, Contract No.: 295322, Virtual nanotitanium: theoretical analysis, design and virtual testing of biocompatibility and mechanical properties of titanium-based nanomaterials, FP7, 1/2014.

- [33] L. Mishnaevsky Jr., E. Levashov, R.Z. Valiev, J. Segurado, I. Sabirov, N. Enikeev, S. Prokoshkin, A.V. Solov'yov, A. Korotitskiy, E. Gutmanas, I. Gotman, E. Rabkin, S. Psakh'e, L. Dluhoš, M. Seefeldt, A. Smolin, Nanostructured titanium-based materials for medical implants: modeling and development, *Mater. Sci. Eng. R* 81 (2014) 1.
- [34] I. Sabirov, M.T. Perez-Prado, J.M. Molina-Aldareguia, I.P. Semenova, G.K. Salimgareeva, R.Z. Valiev, Anisotropy of mechanical properties in high-strength ultra-fine-grained pure Ti processed via a complex severe plastic deformation route, *Scr. Mater.* 64 (2011) 69–72.
- [35] I.P. Semenova, G.V. Klevtsov, N.A. Klevtsova, G.S. Dyakonov, A.A. Matchin, R.Z. Valiev, Nanostructured titanium for maxillofacial mini-implants, *Adv. Eng. Mater.* 18 (7) (2016) 1216–1224.
- [36] C. Arnold, D. Hrušák, L. Dluhoš, Nanoimplantáty—vlastnosti a indikace, StomaTeam CZ, 200726–30 (Nanoimplants—Properties and Indications).
- [37] D. Hrušák, V. Březina, L. Dluhoš, In: Biological properties of nano-titanium, Central European Symposium “VIII Brno implantology days”, Brno, 2006, p. 18.
- [38] V. Březina. Test report no. 31a, surface colonization test. B.P. Medical, Brno, 2011.
- [39] D. Hrušák, L. Dluhoš, et al. In: Biological properties of nanostructured titanium made SPD, XIX Congress of the European Association for Cranio-Maxio-facial Surgery, Bologna, Italy. Sept. 9th–12th 2008. *Abstrakt Journal of Cranio-Maxillofacial Surgery*, Vol. 36, 2008. Supplement 1, s. S260.
- [40] B. An, Z. Li, X. Diao, H. Xin, Q. Zhang, X. Jia, Y. Wu, K. Li, Y. Guo, In vitro and in vivo studies of ultrafine-grain Ti as dental implant material processed by ECAP, *Mater. Sci. Eng. C* 67 (2016) 34–41.
- [41] S. Bagherifard, R. Ghelichi, A. Khademhosseini, M. Guagliano, Cell response to nanocrystallized metallic substrates obtained through severe plastic deformation, *ACS Appl. Mater. Interfaces* 6 (2014) 7963–7985.
- [42] J.W. Park, Y.J. Kim, C.H. Park, D.H. Lee, Y.G. Ko, J.H. Jang, C.S. Lee, Enhanced osteoblast response to an equal channel angular pressing-processed pure titanium substrate with microrough surface topography, *Acta Biomater.* 5 (2009) 3272–3280.
- [43] M. Lai, K. Cai, Y. Hu, X. Yang, Q. Liu, Regulation of the behaviors of mesenchymal stem cells by surface nanostructured titanium, *Colloids Surf. B: Biointerfaces* 97 (2012) 211–220.
- [44] F.L. Nie, Y.F. Zheng, S.C. Wei, D.S. Wang, Z.T. Yu, G.K. Salimgareeva, A.V. Polyakov, R.Z. Valiev, In vitro and in vivo studies on nanocrystalline Ti fabricated by equal channel angular pressing with microcrystalline CP Ti as control, *J. Biomed. Mater. Res. A* 101A (2013) 1694–1707.
- [45] A.V. Polyakov, G.S. Dyakonov, I.P. Semenova, G.I. Raab, L. Dluhos, R.Z. Valiev, Development and study of medical implants made from nanostructured titanium, *Adv Biomat Dev Med* 2 (2015) 63–69.
- [46] C.N. Elias, *Rev. Mater.* 15 (2010) 138.
- [47] X. Liu, P.K. Chu, C. Ding, *Mater. Sci. Eng. R* 47 (2004) 49.
- [48] Z.Q. Yao, Y. Ivanisenko, T. Diemant, A. Caron, A. Chuvilin, J.Z. Jiang, R.Z. Valiev, M. Qi, H.J. Fecht, Synthesis and properties of hydroxyapatite-containing porous titania coating on ultrafine-grained titanium by micro-arc oxidation, *Acta Biomater.* 6 (2010) 2816–2825.
- [49] E.G. Zemtsova, A.Y. Arbenin, R.Z. Valiev, E.V. Orekhov, V.G. Semenov, V.M. Smirnov, Two-level micro-to-nanoscale hierarchical TiO₂ nanolayers on titanium surface, *Materials* 9 (12) (2016) 1010.
- [50] D.V. Nazarov, E.G. Zemtsova, R.Z. Valiev, V.M. Smirnov, Formation of micro-and nanostructures on the nanotitanium surface by chemical etching and deposition of tita-

- nia films by atomic layer deposition (ALD), *Materials* 8 (12) (2015) 8366–8377, <https://doi.org/10.3390/ma80x000x>.
- [51] A. Nanci, J.D. Wuest, L. Peru, P. Brunet, V. Sharma, S. Salzal, M.D. McKee, *J. Biomed. Mater. Res.* 40 (1998) 324.
- [52] Z. Schwartz, J.Y. Martin, D.D. Dean, J. Simpson, D.L. Cochran, B.D. Boyan, *J. Biomed. Mater. Res.* 30 (1996) 145.
- [53] Y. Estrin, C. Kasper, S. Diederichs, R. Lapovok, *J. Biomed. Mater. Res. A* 90 (2009) 1239.
- [54] T.N. Kim, A. Balakrishnan, B.C. Lee, W.S. Kim, K. Smetana, J.K. Park, B.B. Panigrahi, *Biomed. Mater.* 2 (2007) 117.
- [55] S. Faghihi, A.P. Zhilyaev, J.A. Szpunar, F. Azari, H. Vali, M. Tabrizian, *Adv. Mater.* 19 (2007) 1069.
- [56] C. Yao, E.B. Slamovich, J. Qazi, H.J. Rack, T.J. Webster, *Ceram. Trans.* 159 (2005) 239.
- [57] T.N. Kim, A. Balakrishnan, B.C. Lee, W.S. Kim, B. Dvorankova, K. Smetana, J.K. Park, B.B. Panigrahi, *J. Mater. Sci. Mater. Med.* 19 (2008) 553.
- [58] E-466-96 Standard Practice for Conducting Force Controlled Constant Amplitude Axial Fatigue Tests of Metallic Materials.
- [59] C.N. Elias, *Review, Expert. Rev. Med. Devices* 7 (2) (2010) 241.
- [60] ISO 4287—Geometrical Product Specifications (GPS)—Surface Texture: Profile method—Term, Definitions and Surface Texture Parameters. Inter Organization for Standardization, 2009, p. 42.
- [61] A. Balyanov, J. Kutnyakova, N.A. Amirkhanova, V.V. Stolyarov, R.Z. Valiev, X.Z. Liao, Y.H. Zhao, Y.B. Jiang, H.F. Xu, T.C. Lowe, Y.T. Zhu, *Scr. Mater.* 51 (2004) 225.
- [62] D.V. Nazarov, E.G. Zemtsova, A.Y. Solokhin, R.Z. Valiev, V.M. Smirnov, Modification of the surface topography and composition of ultrafine and coarse grained titanium by chemical etching, *Nano* 7 (2017) 15.
- [63] E. Matykina, R. Arrabal, R.Z. Valiev, J.M. Molina-Aldareguia, P. Belov, I. Sabirov, Electrochemical anisotropy of nanostructured titanium for biomedical implants, *Electrochim. Acta* 176 (2015) 1221–1232.
- [64] H.S. Hafez, E.M.N. Selim, F.H. Kamel Eid, W.A. Tawfik, E.A. Al-Ashkar, Y.A. Mostafa, *Am. J. Orthod. Dentofac. Orthop.* 140 (2011) 298–308.
- [65] M.G. Blaya, D.S. Blaya, P. Mello, E.M.M. Flores, L.M. Hirakata, *Revista Odonto Ciencia, Acta Biomater.* 10 (2014). 2379-2324.
- [66] J.C.E. Odekerken, T.J.M. Welting, J.J.C. Arts, G.H.I.M. Walenkamp, P.J. Emans, in: M. Aliofkhaezraeli (Ed.), *Modern Surface Engineering Treatments*, In Tech, New York, 2013, pp. 45–73.
- [67] B.G. Zhang, D.E. Myers, G.G. Wallace, et al., *Int. J. Mol. Sci.* 15 (2014) 11878–11921.
- [68] S.V. Dorozhkin, *Mater. Sci. Eng. C Mater. Biol. Appl.* 55 (2015) 272–326.
- [69] S. Wu, X. Liu, K.W.K. Yeung, et al., *Mater. Sci. Eng. R. Rep.* 80 (2014) 1–36.
- [70] A. Lugovskoy, S. Lugovskoy, *Mater. Sci. Eng. C Mater. Biol. Appl.* 43 (2014) 527–532.
- [71] E. Mohseni, E. Zalnezhad, A.R. Bushroa, *Int. J. Adhes. Adhes.* 48 (2014) 238–257.
- [72] A.L. Yerokhin, X. Nie, A. Leyland, et al., *Surf. Coat. Technol.* 122 (1999) 73–93.
- [73] M. Mohedano, R. Guzman, R. Arrabal, et al., *J. Biomed. Mater. Res. B Appl. Biomater.* 101 (2013) 1524–1537.
- [74] Y. Wang, H. Yu, C. Chen, et al., *Mater. Des.* 85 (2015) 640–652.
- [75] E.V. Legostaeva, Y.P. Sharkeev, M. Eppele, et al., *Russ. Phys. J.* 56 (2014) 1130–1136.
- [76] E.V. Parfenov, A. Yerokhin, A. Matthews, *Surf. Coat. Technol.* 203 (2009) 2896–2904.
- [77] E.V. Parfenov, A. Yerokhin, R.R. Nevyantseva, et al., *Surf. Coat. Technol.* 269 (2015) 2–22.

- [78] Z.Q. Yao, Y. Ivanisenko, T. Diemant, et al., *Acta Biomater.* 6 (2010) 2816–2825.
- [79] A. Aslaran, G. Purcek, I. Hacisalihoglu, et al., *Surf. Coat. Technol.* 205 (2011) S537–S542.
- [80] Y.P. Sharkeev, E.V. Legostaeva, Y.A. Eroshenko, et al., *Compos. Interfaces* 16 (2009) 535–546.
- [81] E. Matykina, G. Doucet, F. Monfort, et al., *Electrochim. Acta* 51 (2006) 4709–4715.
- [82] R.H.U. Khan, A.L. Yerokhin, A. Matthews, *Philos. Mag.* 88 (2008) 795–807.
- [83] C.S. Dunleavy, I.O. Golosnoy, J.A. Curran, et al., *Surf. Coat. Technol.* 203 (2009) 3410–3419.
- [84] A. Yerokhin, E.V. Parfenov, A. Matthews, *Surf. Coat. Technol.* 301 (2016) 54–62.
- [85] S.V. Gnedenkov, Y.P. Scharkeev, S.L. Sinebryukhov, et al., *Inorg. Mater. Appl. Res.* 2 (2011) 474–481.
- [86] W.K. Yeung, G.C. Reilly, A. Matthews, et al., *J. Biomed. Mater. Res. B Appl. Biomater.* 101 (2013) 939–949.
- [87] A. Kazek-Kesik, M. Krok-Borkowicz, E. Pamula, et al., *Mater. Sci. Eng. C Mater. Biol. Appl.* 43 (2014) 172–181.
- [88] D. Dzhurinskiy, Y. Gao, W.K. Yeung, et al., *Surf. Coat. Technol.* 269 (2015) 258–265.
- [89] X. Lu, M. Mohedano, C. Blawert, et al., *Surf. Coat. Technol.* 307 (2016) 1165–1182.
- [90] A.R. Rafieerad, M.R. Ashra, R. Mahmoodian, et al., *Mater. Sci. Eng. C Mater. Biol. Appl.* 57 (2015) 397–413.
- [91] O.P. Terleeva, Y.P. Sharkeev, A.I. Slonova, et al., *Surf. Coat. Technol.* 205 (2010) 1723–1729.
- [92] C.J. Chung, R.T. Su, H.J. Chu, et al., *J. Biomed. Mater. Res. B Appl. Biomater.* 101 B (2013) 1023–1030.